PRAMANA
— journal of
physics

Vol. 58, No. 4
April 2002
pp. 669–684

Cross-phase modulational instability in an elliptical birefringent fiber with higher order nonlinearity and dispersion

R GANAPATHY and V C KURIAKOSE
Department of Physics, Cochin University of Science and Technology, Kochi 682 022, India
Email: ganapathyr@cusat.ac.in; vck@cusat.ac.in

MS received 18 December 2001

Abstract. We obtain conditions for the occurrence of cross-phase modulational instability in the normal dispersion regime for the coupled higher order nonlinear Schrödinger equation with higher order dispersion and nonlinear terms.

Keywords. Cross-phase modulational instability; normal dispersion; group velocity mismatch; birefringent optical fiber.

PACS Nos 42.81.Gs; 42.65.Sf; 42.65.Tg

1. Introduction

A continuous wave with a cubic nonlinearity in an anomalous dispersion regime is known to develop instability with respect to small modulations in amplitude or in phase, called modulational instability (MI) [1]. The MI phenomenon was discovered in fluids [2], in nonlinear optics [3] and in plasmas [4]. MI of a light wave in an optical fiber was suggested by Hasegawa and Brinkman [5] as a means to generate a far infrared light source and since then has attracted extensive attention for both its fundamental and applied interests [1]. As regards applications, MI provides a natural means of generating ultrashort pulses at ultrahigh repetition rates and is thus potentially useful for the development of high speed optical communication systems in future [1,6,7] and hence has been exploited a great deal in many theoretical and experimental studies for the realization of laser sources adapted to ultrahigh bit-rate optical transmissions. MI phenomenon is accompanied by side-band evolution at a frequency separation from the carrier which is proportional to the optical pump power [1,6,7]. When two or more optical waves copropagate through a birefringent optical fiber, they interact with each other through the fiber nonlinearity in such a way that the effective refractive index of a wave depends not only on the intensity of that wave but also on the intensity of other copropagating waves, a phenomenon known as cross-phase modulation (XPM) [1,6–8]. MI in a birefringent optical fiber can be experimentally observed via two techniques, namely, the single-frequency copropagation where

two pump waves of identical frequency copropagate with orthogonal polarizations parallel to the two birefringence axes of the fiber [9] and the two-frequency copropagation, where the two polarized wave copropagate with different frequencies [9]. Drummond, Kennedy and Harvey have demonstrated experimentally that MI can occur for the normal dispersion regime by using the single frequency copropagation technique [10] and have pointed out that the appearance of MI in the normal dispersion regime for a highly birefringent fiber is due to the group velocity mismatch (GVM) between the two copropagating waves and termed the instability as cross-phase MI (XMI) [10]. When breakup of continuous wave and quasi-continuous wave radiates into a train of picosecond and femto second pulses in the fiber, higher order dispersion effects such as self-steepening, self-induced Raman scattering (SRS) and higher order dispersion effects such as third- and fourth-order dispersion should also be taken into account [6–8]. In an earlier work we have considered the influence of fourth-order dispersion effect alone when considering the occurrence of polarization modulation instability of ultrashort pulses of 500 fs and above on a circularly birefringent optical fiber [11] without considering group velocity mismatch. We arrived at the conclusion that the slow and the fast axes of a polarization preserving fiber are not equivalent when one considers the influence due to fourth-order dispersion effect also. In the present paper, we study the influence of cross-phase modulation (XPM), higher order nonlinear effects such as self-steepening, self-induced Raman scattering (SRS) and higher order dispersion effects such as third- and fourth-order dispersion on XMI for a highly elliptical birefringent optical fiber and obtain conditions for the occurrence of XMI in the normal dispersion regime.

The paper is arranged as follows: In §2, we briefly discuss the basic equation. MI conditions for the basic equation are determined in §3. In §4 we present the derivation of the coupled linearized equations for the four side-band amplitudes in the two orthogonal linear polarization components of the pump wave, arrive at the MI conditions and compare the results with those in §3. In §5, we conclude.

2. Basic equation

We consider coupled higher order nonlinear Schrödinger equation (CHNSE) model [6–8] with the addition of self-steepening, SRS, third- and fourth-order dispersion effects given by

$$\begin{aligned}
&\mathrm{i}\left(U_z+\frac{\delta}{2}U_T\right)-\frac{\beta_2}{2}U_{TT}+\gamma\left(|U|^2+B|V|^2\right)U-\mathrm{i}\frac{\beta_3}{6}U_{TTT}-\frac{\beta_4}{24}U_{TTTT}+\\
&\mathrm{i}\frac{\gamma}{\omega_0}\left[\left(\varepsilon_1'|U|^2+\varepsilon_2'|V|^2\right)U\right]_T-\gamma\left(U\left[\varepsilon_3'|U|^2+\varepsilon_4'|V|^2\right]_T+\varepsilon_5'V\left[UV^*\right]_T\right)=0,\\
&\mathrm{i}\left(V_z-\frac{\delta}{2}V_T\right)-\frac{\beta_2}{2}V_{TT}+\gamma\left(B|U|^2+|V|^2\right)V-\mathrm{i}\frac{\beta_3}{6}V_{TTT}-\frac{\beta_4}{24}V_{TTTT}+\\
&\mathrm{i}\frac{\gamma}{\omega_0}\left[\left(\varepsilon_2'|U|^2+\varepsilon_1'|V|^2\right)V\right]_T-\gamma\left(V\left[\varepsilon_4'|U|^2+\varepsilon_3'|V|^2\right]_T+\varepsilon_5'U\left[U^*V\right]_T\right)=0,
\end{aligned}\tag{1}$$

where z is the longitudinal distance, $T=t-(z/v_g)$ is the retarded time and β_2,β_3 and β_4 are the second-, third- and fourth-order dispersion coefficients respectively. The terms in

the first square parenthesis denote the effect due to self-steepening [6–8,12]. ε_1' and ε_2' are constants and are the coefficients of the self-steepening terms. The terms in the last parenthesis are instrumental for the occurrence of SRS [6–8,13]. ε_3', ε_4' and ε_5' represent the coefficients of SRS and are related to each other via the equation $\varepsilon_3' = \varepsilon_4' + \frac{2\cos^2(\theta)}{1+\sin^2(\theta)}\varepsilon_5'$ where θ is the ellipticity angle [13].

In the dimensionless form, the above equation becomes

$$\begin{aligned}
&\mathrm{i}\left(u_\zeta' + \Delta u_\tau'\right) - S_1 u_{\tau\tau}' + \left[\left|u'\right|^2 + B\left|v'\right|^2\right] u' - \mathrm{i}S_2 u_{\tau\tau\tau}' - S_3 u_{\tau\tau\tau\tau}' + \\
&\mathrm{i}\left[\left(\varepsilon_1\left|u'\right|^2 + \varepsilon_2\left|v'\right|^2\right)u'\right]_\tau - \left(u'\left[\varepsilon_3\left|u'\right|^2 + \varepsilon_4\left|v'\right|^2\right]_\tau + \varepsilon_5 v'\left[u'v'^*\right]_\tau\right) = 0, \\
&\mathrm{i}\left(v_\zeta' - \Delta v_\tau'\right) - S_1 v_{\tau\tau}' + \left[B\left|u'\right|^2 + \left|v'\right|^2\right] v' - \mathrm{i}S_2 v_{\tau\tau\tau}' - S_3 v_{\tau\tau\tau\tau}' + \\
&\mathrm{i}\left[\left(\varepsilon_2\left|u'\right|^2 + \varepsilon_1\left|v'\right|^2\right)v'\right]_\tau - \left(v'\left[\varepsilon_4\left|u'\right|^2 + \varepsilon_3\left|v'\right|^2\right]_\tau + \varepsilon_5 u'\left[u'^* v'\right]_\tau\right) = 0,
\end{aligned} \tag{2}$$

where $\varsigma = \frac{z}{T_0^2}|\beta_2|$, $\tau = \frac{T}{T_0}$, $\Delta = \frac{T_0^\delta}{2|\beta_2|}$, $S_1 = \frac{s_1}{2}$, $S_2 = \frac{s_2|\beta_3|}{6T_0|\beta_2|}$, $S_3 = \frac{s_3|\beta_4|}{24T_0^2|\beta_2|}$, $U = \sqrt{\frac{|\beta_2|}{\gamma T_0^2}}u'$, $V = \sqrt{\frac{|\beta_2|}{\gamma T_0^2}}v'$, $\varepsilon_1 = \frac{\varepsilon_1'}{\omega_0 T_0}$, $\varepsilon_2 = \frac{\varepsilon_2'}{\omega_0 T_0}$, $\varepsilon_3 = \frac{\varepsilon_3'}{T_0}$, $\varepsilon_4 = \frac{\varepsilon_4'}{T_0}$, $\varepsilon_5 = \frac{\varepsilon_5'}{T_0}$, where T_0 is an arbitrary time scale which is π, the initial pulse width. In this work we consider three different scenario for generation of ultrashort pulses of various pulse widths, governed by the respective MI conditions: (i) generation of ultrashort pulses of the order of 500 fs and above [14] where all the higher order nonlinear terms can be neglected [15,16], i.e., $\varepsilon_1 = \varepsilon_2 = \varepsilon_3 = \varepsilon_4 = \varepsilon_5 = 0$ with only the third- and fourth-order dispersion terms remaining in eq. (2). In an earlier work we have considered this case after neglecting the group velocity mismatch parameter Δ [11]; (ii) generation of ultrashort pulses in the femto second region below 500 fs where the influence of SRS and self-steepening should also be considered along with the higher order dispersion terms [6–8]; (iii) generation of ultrashort pulses in the sub-pico femto second region where both the self-steepening and fourth-order dispersion terms can be safely neglected [6–8].

3. Modulational instability conditions

Equation (2) admits steady state solutions of the form

$$\begin{aligned}
u' &= \sqrt{P_1}\exp\left(\mathrm{i}\zeta\left(P_1 + BP_2\right)\right), \\
v' &= \sqrt{P_2}\exp\left(\mathrm{i}\zeta\left(P_2 + BP_1\right)\right),
\end{aligned} \tag{3}$$

where $P_{1,2}$ are proportional to input powers along the principal axes. We examine the stability of the steady state solution by looking into the system in the presence of small amplitude perturbations u and v given by

$$\begin{aligned}
u' &= \left(\sqrt{P_1} + u\right)\exp\left(\mathrm{i}\zeta\left(P_1 + BP_2\right)\right), \\
v' &= \left(\sqrt{P_2} + v\right)\exp\left(\mathrm{i}\zeta\left(P_2 + BP_1\right)\right).
\end{aligned} \tag{4}$$

On substituting eq. (4) into eq. (2) and on linearizing about u and v, we obtain the following linearized equations in u and v:

$$\begin{aligned}
&\mathrm{i}\left(u_\zeta+\Delta u_\tau\right)-S_1u_{\tau\tau}+\left(P_1\left(u+u^*\right)+B\sqrt{P_1P_2}\left(v+v^*\right)\right)-\mathrm{i}S_2u_{\tau\tau\tau}-S_3u_{\tau\tau\tau\tau}\\
&\qquad+\mathrm{i}\left(\varepsilon_1P_1\left[u^*+2u\right]_\tau+\varepsilon_2\left[P_2u+\sqrt{P_1P_2}\left(v+v^*\right)\right]_\tau\right)\\
&\qquad-\left(\varepsilon_3P_1\left[u+u^*\right]_\tau+\varepsilon_4\sqrt{P_1P_2}\left[v+v^*\right]_\tau+\varepsilon_5\left[P_2u+\sqrt{P_1P_2}v^*\right]_\tau\right)=0,\\
&\mathrm{i}\left(v_\zeta-\Delta v_\tau\right)-S_1v_{\tau\tau}+\left(B\sqrt{P_1P_2}\left(u+u^*\right)+P_2\left(v+v^*\right)\right)-\mathrm{i}S_2v_{\tau\tau\tau}-S_3v_{\tau\tau\tau\tau}\\
&\qquad+\mathrm{i}\left(\varepsilon_1P_2\left[v^*+2v\right]_\tau+\varepsilon_2\left[P_1v+\sqrt{P_1P_2}\left(u+u^*\right)\right]_\tau\right)\\
&\qquad-\left(\varepsilon_3P_2\left[v+v^*\right]_\tau+\varepsilon_4\sqrt{P_1P_2}\left[u+u^*\right]_\tau+\varepsilon_5\left[\sqrt{P_1P_2}u^*+P_1v\right]_\tau\right)=0,
\end{aligned}\tag{5}$$

where we have considered the case for a linearly polarized pump oriented at arbitrary angles with respect to either the slow or the fast axis [1,6]. On Fourier transforming the linearized equations given by eq. (5), according to the relations

$$\begin{aligned}
A_1\left(\zeta,\omega\right)&=\frac{1}{\sqrt{2\pi}}\int_{-\infty}^{+\infty}u\left(\zeta,\tau\right)\exp\left(\mathrm{i}\omega\tau\right)\mathrm{d}\tau,\\
A_2\left(\zeta,\omega\right)&=\frac{1}{\sqrt{2\pi}}\int_{-\infty}^{+\infty}v\left(\zeta,\tau\right)\exp\left(\mathrm{i}\omega\tau\right)\mathrm{d}\tau,
\end{aligned}\tag{6}$$

we obtain four linearized equations in terms of $A_1+A_1^\dagger$, $A_1-A_1^\dagger$, $A_2+A_2^\dagger$ and $A_2-A_2^\dagger$ which are of the form

$$\begin{aligned}
\mathrm{i}\frac{\partial\left(A_1+A_1^\dagger\right)}{\partial\zeta}&=M_{11}\left(A_1+A_1^\dagger\right)+M_{12}\left(A_1-A_1^\dagger\right)+M_{13}\left(A_2+A_2^\dagger\right)+M_{14}\left(A_2-A_2^\dagger\right),\\
\mathrm{i}\frac{\partial\left(A_1-A_1^\dagger\right)}{\partial\zeta}&=M_{21}\left(A_1+A_1^\dagger\right)+M_{22}\left(A_1-A_1^\dagger\right)+M_{23}\left(A_2+A_2^\dagger\right)+M_{24}\left(A_2-A_2^\dagger\right),\\
\mathrm{i}\frac{\partial\left(A_2+A_2^\dagger\right)}{\partial\zeta}&=M_{31}\left(A_1+A_1^\dagger\right)+M_{32}\left(A_1-A_1^\dagger\right)+M_{33}\left(A_2+A_2^\dagger\right)+M_{34}\left(A_2-A_2^\dagger\right),\\
\mathrm{i}\frac{\partial\left(A_2-A_2^\dagger\right)}{\partial\zeta}&=M_{41}\left(A_1+A_1^\dagger\right)+M_{42}\left(A_1-A_1^\dagger\right)+M_{43}\left(A_2+A_2^\dagger\right)+M_{44}\left(A_2-A_2^\dagger\right),
\end{aligned}$$

where $M_{11}=\Delta\omega+S_2\omega^3+P\omega\left(3\varepsilon_1+\varepsilon_2\right)$, $M_{12}=S_1\omega^2-S_3\omega^4+\mathrm{i}\varepsilon_5P\omega$, $M_{13}=2\varepsilon_2P\omega$, $M_{14}=-\mathrm{i}\varepsilon_5P\omega$, $M_{21}=S_1\omega^2-S_3\omega^4+2P+\mathrm{i}P\omega\left(2\varepsilon_3+\varepsilon_5\right)$, $M_{22}=\Delta\omega+S_2\omega^3+P\omega\left(\varepsilon_1+\varepsilon_2\right)$, $M_{23}=2BP+\mathrm{i}P\omega\left(\varepsilon_4+\varepsilon_5\right)$, $M_{31}=2\varepsilon_2P\omega$, $M_{32}=-\mathrm{i}\varepsilon_5P\omega$, $M_{33}=-\Delta\omega+S_2\omega^3+P\omega\left(3\varepsilon_1+\varepsilon_2\right)$, $M_{34}=M_{12}$, $M_{41}=2BP+\mathrm{i}P\omega\left(2\varepsilon_4+\varepsilon_5\right)$, $M_{43}=M_{21}$, $M_{44}=-\Delta\omega+S_2\omega^3+P\omega\left(\varepsilon_1+\varepsilon_2\right)$. We have also considered the relation $A_1^\dagger\left(\varsigma,\omega\right)=\left[A_1\left(\varsigma,-\omega\right)\right]^*$ and $A_2^\dagger\left(\varsigma,\omega\right)=\left[A_2\left(\varsigma,-\omega\right)\right]^*$ where the asterix denotes complex conjugate. These equations can be brought into the following matrix form:

$$\mathrm{i}\frac{\partial\mathbf{A}\left(\varsigma,\omega\right)}{\partial\zeta}=-\mathbf{M}\left(\omega\right)\mathbf{A}\left(\varsigma,\omega\right)\tag{7}$$

where

$$\mathbf{A}(\varsigma,\omega)=\begin{pmatrix} A_1+A_1^{\dagger} \\ A_1-A_1^{\dagger} \\ A_2+A_2^{\dagger} \\ A_2-A_2^{\dagger} \end{pmatrix}, \tag{8}$$

and

$$\mathbf{M}(\omega)=\begin{pmatrix} M_{11} & M_{12} & M_{13} & M_{14} \\ M_{21} & M_{22} & M_{23} & 0 \\ M_{31} & M_{32} & M_{33} & M_{34} \\ M_{41} & 0 & M_{43} & M_{44} \end{pmatrix}. \tag{9}$$

The eigenvalue equation is given by

$$|M(\omega)-kI|=0, \tag{10}$$

where I is the identity matrix. From eq. (10) we obtain a dispersion relation in k which is a fourth-order polynomial equation. MI occurs when there is an exponential growth in the amplitude of the perturbed wave which implies the existence of a nonvanishing imaginary part in the complex eigenvalue k [1,6–8,10]. The importance of the MI phenomenon is measured by a gain given by $G=|\mathrm{Im}\,k|$ where $\mathrm{Im}\,k$ denotes the imaginary part of k. We next investigate the MI conditions for various regimes of pulse propagation. We now discuss the results obtained for the three different cases mentioned in §2.

(i) *MI condition governing the generation of ultrashort pulses in the femto second region of the order of 500 fs and above*

This scenario has been experimentally studied by Cavalacanti *et al* for the scalar nonlinear Schrödinger equation [14]. We now consider the case when the linearly polarized pump is oriented at 45° with respect to both the axes such that equal power is distributed along each axis, i.e., $P_1=P_2=P$ with the total input power being $2P$. From eq. (10), we obtain the dispersion relation between k and ω which is of the form

$$k^4-4S_2\omega^3k^3-2\omega^2L_1k^2+4S_2\omega^5L_2k+\omega^4L_3=0 \tag{11}$$

where

$$\begin{aligned}
L_1 &= \Delta^2+\omega^2\left(S_1^2-3S_2^2\omega^2+S_3^2\omega^4\right)-S_1\left(2S_3\omega^4-P\right), \\
L_2 &= \Delta^2+\omega^2\left(S_1^2-S_2^2\omega^2+S_3^2\omega^4-S_3P\right)-S_1\left(2S_3\omega^4-P\right), \\
L_3 &= \Delta^4+\omega^4\left(-S_2^2\omega^2+\left(S_1-S_3\omega^2\right)^2\right)^2+\left(1-B^2\right)\left(S_1-S_3\omega^2\right)^2P^2 \\
&\quad +2\omega^2\left(S_1-S_3\omega^2\right)\left(-S_2^2\omega^2+\left(S_1-S_3\omega^2\right)^2\right)P \\
&\quad -2\Delta^2\left(\omega^2\left(S_1^2+S_2^2\omega^2+S_3^2\omega^4-S_3P\right)-S_1\left(2S_3\omega^4-P\right)\right)
\end{aligned}$$

$S_1=-\frac{1}{2}$ portrays the case of MI in the anomalous dispersion regime which has been discussed in detail in refs [1,11,12]. We now consider the normal dispersion regime denoted

by $S_1 = \frac{1}{2}$. In this case, the complex eigenvalue k obtained from the dispersion relation given by eq. (11) has the form

$$k = S_2\omega^3 \pm \omega\sqrt{L_4 \pm 2\sqrt{L_5}} \tag{12}$$

where

$$L_4 = \Delta^2 + \left(S_1 - S_3\omega^2\right)\left(S_1\omega^2 - S_3\omega^4 + 2P\right),$$
$$L_5 = \left(S_1 - S_3\omega^2\right)\left(B^2\left(S_1 - S_3\omega^2\right)P^2 + \Delta^2\left(S_1\omega^2 - S_3\omega^4 + 2P\right)\right).$$

Equation (12) is found to possess a nonzero imaginary part only for the case given by

$$k = S_2\omega^3 \pm \omega\sqrt{L_4 - 2\sqrt{L_5}}. \tag{13}$$

Hence from the above equation, we obtain the condition for instability to occur to be $L_4^2 < 4L_5$. From eq. (13) it is clear that the instability condition is not affected irrespective of the presence or absence of S_2, the dimensionless third-order dispersion coefficient. Figure 1 shows the graphical relation between the frequency detuning ω, input power P and gain G for $B = \frac{2}{3}$ which depicts linear birefringence, $\Delta = 3.92512$, $S_1 = 0.5$, $S_2 = 2.6087 \times 10^{-6}$ and $S_3 = 1.69082 \times 10^{-6}$. This corresponds to the case when $|\beta_2| = 69.0$ ps^2/Km, $|\beta_3| = 0.54 \times 10^{-3}$ ps^3/Km and $|\beta_4| = 7.0 \times 10^{-4}$ ps^4/Km. From the graph, it is evident that as the pump power is increased, the peaks of the gain curve move closer to the zero detuning frequency with the peak position changing relatively slowly when compared to

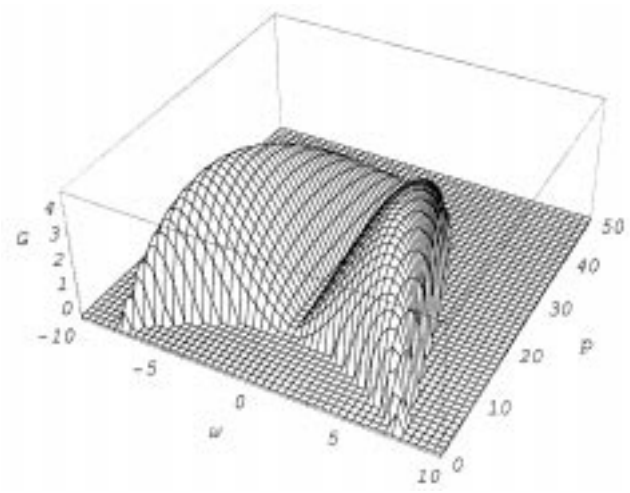

Figure 1. The surface plot for power gain G, frequency detuning ω and input power P for $\Delta = 3.925$, $S_1 = 0.5$, $S_2 = 2.6087 \times 10^{-6}$ and $S_3 = 1.69082 \times 10^{-6}$ and $\varepsilon_1 = \varepsilon_2 = \varepsilon_3 = \varepsilon_4 = \varepsilon_5 = 0$. This corresponds to the case when $|\beta_2| = 69.0$ ps^2/Km, $|\beta_3| = 0.54 \times 10^{-3}$ ps^3/Km and $|\beta_4| = 7.0 \times 10^{-4}$ ps^4/Km.

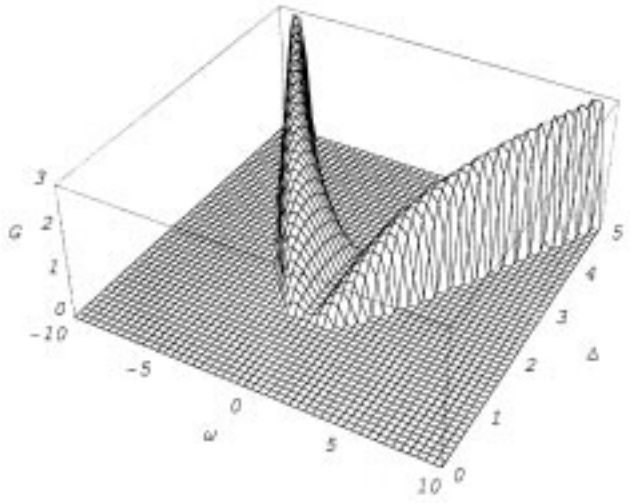

Figure 2. The surface plot for power gain G, frequency detuning ω and group velocity mismatch Δ for $P = 5.0$. The rest parameters have the same values as in figure 1.

the increase in the gain band width. This is the case of cross-phase MI (XMI) which occurs at a finite detuning from the carrier frequency [10]. A marked difference of the present results from the results obtained in ref. [10] is that generation of ultrashort pulses of the order of 500 fs and above requires a comparatively much wider range of input power and the region of MI spreads over a comparatively wider range of the frequency detuning ω, where the fourth-order dispersion plays a dominant role. In figure 2, which shows the graphical relation between gain G, group velocity mismatch Δ and frequency detuning ω for $P = 5.0$ and with the other parameters having the same values as in figure 1, we note that the instability occurs only for finite values of group velocity mismatch. As is well-known, the XPM coupling factor B depends on the ellipticity angle θ and can vary from $\frac{2}{3}$ to 2 for values of θ in the range 0 to $\frac{\pi}{2}$ [1]. $\theta = 0$ corresponds to linear birefringence for which $B = \frac{2}{3}$ and $\theta = \frac{\pi}{2}$ corresponds to circular birefringence for which $B = 2$ [1]. For $\theta \approx 35^\circ$, $B = 1.0$ which corresponds to the ideal birefringence case where the self and cross-phase coupling terms are identical [1]. Figure 3 shows the variation of gain G with respect to the frequency detuning ω and the ellipticity angle θ for $P = 5.0$. In this case, the peaks of the gain curve increase with increasing θ. Furthermore, it can be observed that as the pump power is steadily increased, the gap between the two sidebands decreases and finally approaches the zero detuning frequency. To study the effect of variations in the pump polarization wherein the pump power is not distributed equally along both the axes, we write the pump powers in terms of the polarization angle ϕ, i.e., $P_1 = 2P\cos^2(\phi)$ and $P_2 = 2P\sin^2(\phi)$ such that the total pump power is always equal to $2P$. On substituting these into the eigenvalue eq. (10) we numerically determine the MI condition. Figure 4 depicts the surface plot of the gain spectrum as a function of the frequency detuning ω and the polarization angle ϕ. As in ref. [10], here too maximum gain occurs at $\phi = 45^\circ$ and no XMI is observed when the linearly polarized pump is polarized on either principal axis.

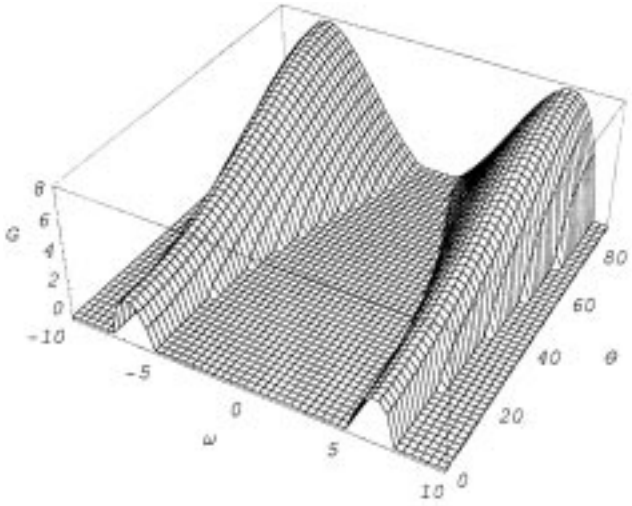

Figure 3. The surface plot for power gain G, frequency detuning ω and ellipticity angle θ for the same values as in figure 2.

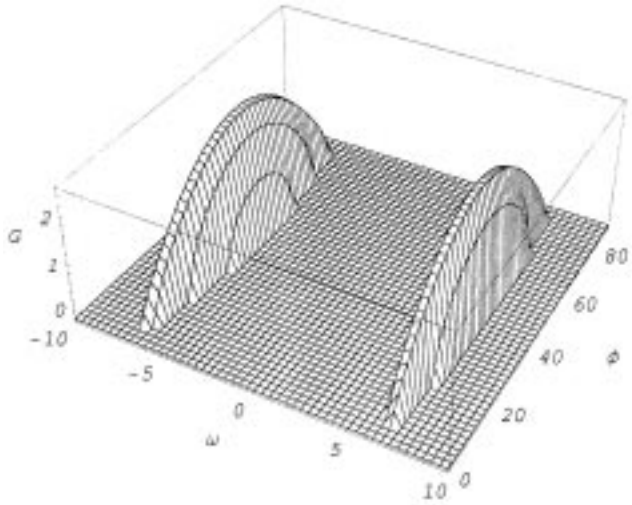

Figure 4. The surface plot for power gain G, frequency detuning ω and polarization angle ϕ for the same values as in figure 2.

(ii) *MI condition governing the generation of ultrashort pulses in the femto second region below 500 fs*

It is not possible to neglect the influence of SRS and self-steepening on the MI in this regime. For the same values of the dispersion parameters as considered in figure 1 and with $\Delta = 1.963$, $S_1 = 0.5$, $S_2 = 5.217 \times 10^{-6}$, $S_3 = 6.763 \times 10^{-6}$, $\varepsilon_1 = \varepsilon_2 = 4.0 \times 10^{-6}$, $\varepsilon_3 = 0.03$, $\varepsilon_4 = \varepsilon_5 = 0.01$, we determine the XMI condition by numerically evaluating

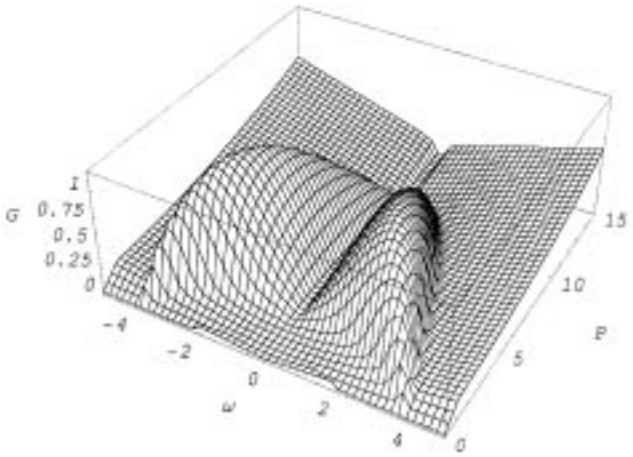

Figure 5. The surface plot for power gain G, frequency detuning ω and input power P for $\Delta = 1.963$, $S_1 = 0.5$, $S_2 = 5.217 \times 10^{-6}$, $S_3 = 6.763 \times 10^{-6}$, $\varepsilon_1 = \varepsilon_2 = 4.0 \times 10^{-6}$, $\varepsilon_3 = 0.03$, $\varepsilon_4 = \varepsilon_5 = 0.01$.

the eigenvalue eq. (10) when the linearly polarized pump is polarized equally with respect to either axis. The corresponding gain spectrum as a function of frequency detuning ω and input power P is portrayed in figure 5. From figure 5, it is evident that for comparatively low values of ω, the gain spectrum is dominated more by XPM and GVD effects with the result that in that specific region we obtain a gain spectrum similar to the case depicted in figure 1. Here too, the occurrence of MI requires a comparatively wider range of input power but lesser than that in case (i). By suitably adjusting the various parameters, we arrive at the inference that while self-steepening reduces the maximum value of the gain spectrum, SRS enhances the region of MI. One effect dominates over the other depending on the values of the various parameters considered in the article. In most cases the SRS dominates over the self-steepening effect. Thus SRS has a hand in reducing the range of input power required for the instability to occur which nullifies to an extent the demand for a comparatively wider range of input power by fourth-order dispersion and self-steepening. As a result, for comparatively higher values of ω and with increasing power, SRS effect becomes predominant with the result that the gain spectrum increases linearly with ω. In a nutshell, the effect of SRS widens the region of MI whereas the effect of self-steepening tries to reduce the maximum gain which is evident when one compares figures 1 and 5. A marked difference between cases (i) and (ii) is that in the latter case, the influence on MI due to the fourth-order dispersion term is much less when compared with the former case. Figures 6–8 which portray the frequency dependent gain as functions of Δ, θ and ϕ respectively for an input power $P = 5.0$, bring forth similar effects of SRS on MI as portrayed in figure 5 with the result that the gain parameter has nonzero values everywhere except for the zero detuning frequency where the gain parameter vanishes.

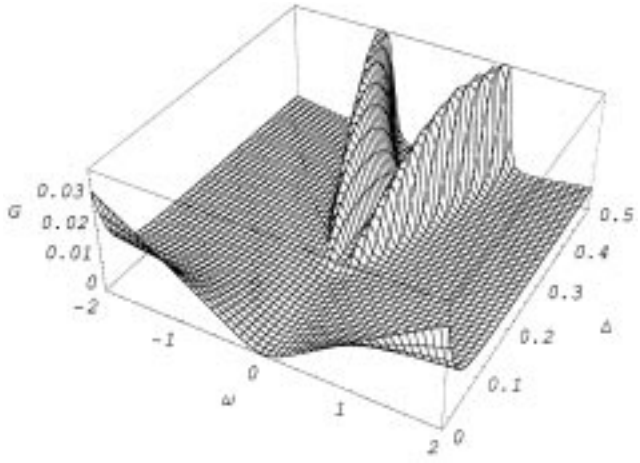

Figure 6. The surface plot for power gain G, frequency detuning ω and group velocity mismatch Δ for $P = 0.1$. The rest parameters have the same values as in figure 5.

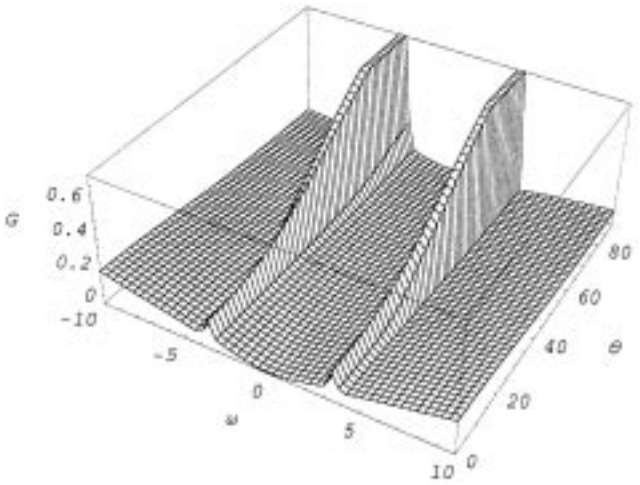

Figure 7. The surface plot for power gain G, frequency detuning ω and ellipticity angle θ for the same values as in figure 6.

(iii) *MI condition governing the generation of ultrashort pulses in the sub-pico-femto second region*

The MI condition which governs the generation of ultrashort pulses in the sub-pico-femto second regime is only influenced by the effect due to SRS and as a result, the effects due to self-steepening and fourth-order dispersion can be safely neglected. Based on this, the gain parameter is plotted in figure 9 as a function of frequency detuning and input power. A marked difference in this case from that in (i) and (ii) is that the instability condition is achieved for a comparatively shorter range of input power. Moreover, SRS enhances

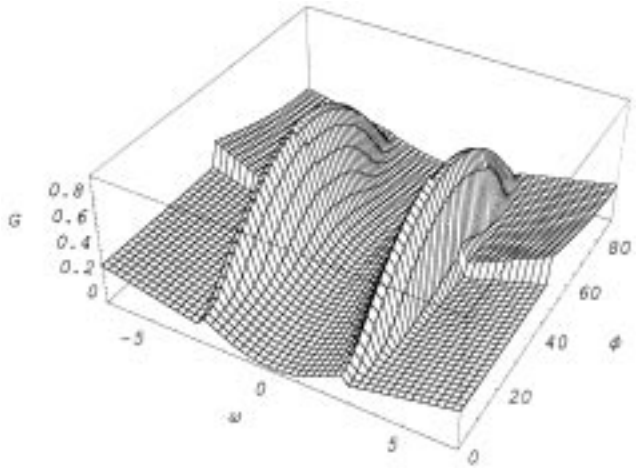

Figure 8. The surface plot for power gain G, frequency detuning ω and polarization angle ϕ for the same values as in figure 6.

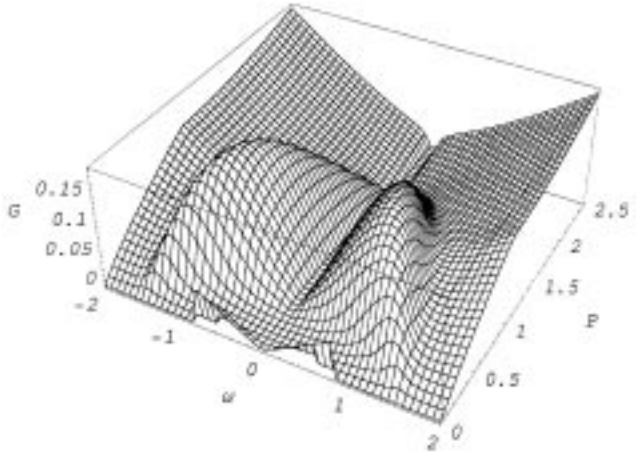

Figure 9. The surface plot for power gain G, frequency detuning ω and input power P for $\Delta = 0.785$, $S_1 = 0.5$, $S_2 = 1.304 \times 10^{-3}$, $S_3 = 0.0$, $\varepsilon_1 = \varepsilon_2 = 0.0$, $\varepsilon_3 = 0.075$, $\varepsilon_4 = \varepsilon_5 = 0.025$.

the region of MI. These are clearly depicted in figures 10–12 which portray the frequency dependent gain as functions of Δ, θ and ϕ respectively for an input power $P = 0.1$. This case is closer to the result obtained in [10].

Figure 13 compares the gain spectrum obtained in case (iii) with that of [10]. Thus we are able to retrieve the result in [10] when the input parameters considered in this article are assigned with the values in [10].

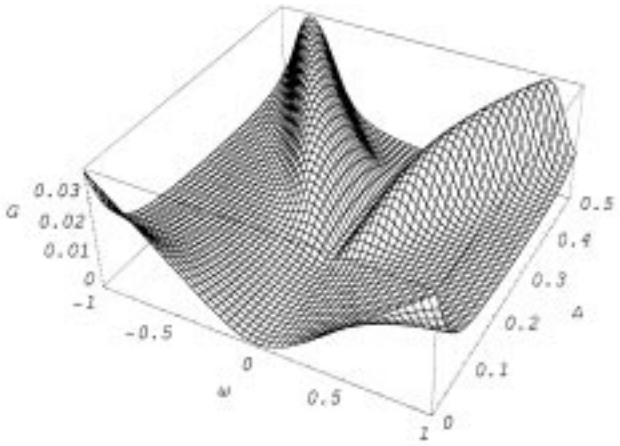

Figure 10. The surface plot for power gain G, frequency detuning ω and group velocity mismatch Δ for $P = 0.1$. The rest parameters have the same values as in figure 9.

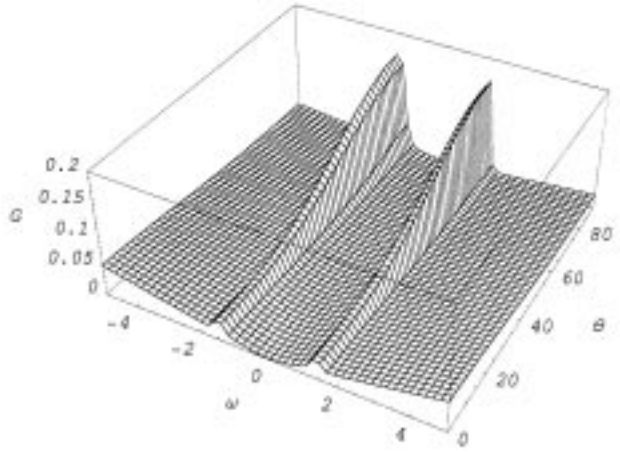

Figure 11. The surface plot for power gain G, frequency detuning ω and ellipticity angle θ for the same values as in figure 10.

4. MI phenomenon in terms of Stokes and anti-Stokes side-band amplitudes

The regions of instability may also be understood as arising from a process in which the group-velocity dispersion of the down shifted side-band polarized on the slow axis and the up-shifted sideband on the fast axis, is balanced by the group velocity mismatch. This can be verified by assuming for perturbation, a modulation anstatz with wave number k and frequency ω of the form

$$u(\varsigma,\tau) = u_s(\varsigma)\exp(\mathrm{i}\omega\tau) + u_a(\varsigma)\exp(-\mathrm{i}\omega\tau),$$
$$v(\varsigma,\tau) = v_s(\varsigma)\exp(\mathrm{i}\omega\tau) + v_a(\varsigma)\exp(-\mathrm{i}\omega\tau), \qquad (14)$$

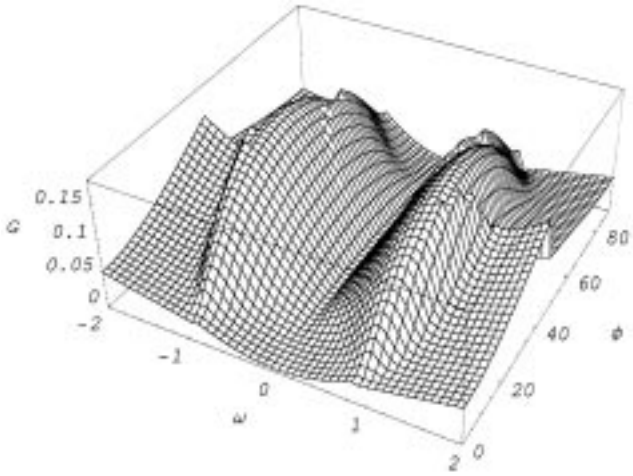

Figure 12. The surface plot for power gain G, frequency detuning ω and polarization angle ϕ for the same values as in figure 10.

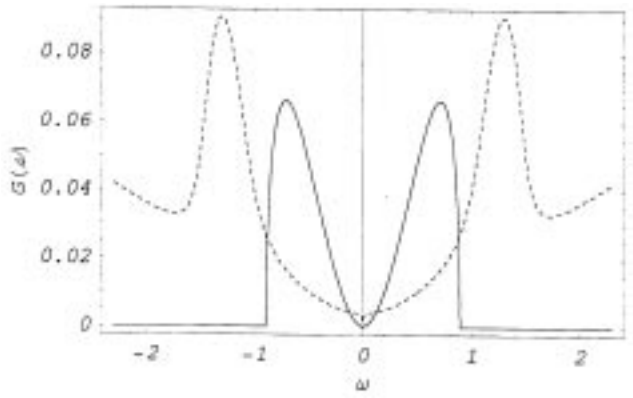

Figure 13. Compares the gain spectrum obtained in case (iii) (dotted line) with that of ref. [10] (solid line) for $P = 0.1$.

where u_s and u_a can be regarded respectively, as the measures of the amplitudes of the Stokes and anti-Stokes sidebands for the slow axis whereas v_s and v_a represent those of the fast axis.

On substituting the above expressions into eq. (2) and on linearizing with respect to u_s, u_a^*, v_s and v_a^*, we finally arrive at a set of coupled linear differential equations in terms of the perturbing fields u_s, u_a^*, v_s and v_a^* which can be written in the form of a matrix equation given by

$$-\mathrm{i}\frac{\mathrm{d}\mathbf{X}(\varsigma)}{\mathrm{d}\varsigma} = \mathbf{L}\,\mathbf{X}(\varsigma) \tag{15}$$

where the column matrix $\mathbf{X}(\varsigma) = \begin{pmatrix} u_s \\ u_a^* \\ v_s \\ v_a^* \end{pmatrix}$ and

$$\mathbf{L} = \begin{pmatrix} L_{11} & L_{12} & L_{13} & L_{14} \\ L_{21} & L_{22} & L_{23} & L_{24} \\ L_{31} & L_{32} & L_{33} & L_{34} \\ L_{41} & L_{42} & L_{43} & L_{44} \end{pmatrix} \tag{16}$$

where the elements of $\mathbf{L}$ take the form

$$\begin{aligned}
L_{11} &= P_1 - \Delta\omega + S_1\omega^2 - S_3\omega^4 - S_2\omega^3 - \omega\left(2\varepsilon_1 P_1 + \varepsilon_2 P_2\right) - \mathrm{i}\omega\left(\varepsilon_3 P_1 + \varepsilon_5 P_2\right), \\
L_{12} &= P_1\left(1 - \varepsilon_1\omega - \mathrm{i}\varepsilon_3\omega\right), \quad L_{13} = \sqrt{P_1P_2}\left(B - \varepsilon_2\omega - \mathrm{i}\varepsilon_4\omega\right), \\
L_{14} &= \sqrt{P_1P_2}\left(B - \varepsilon_2\omega - \mathrm{i}\varepsilon_4\omega - \mathrm{i}\varepsilon_5\omega\right), \quad L_{21} = P_1\left(-1 - \varepsilon_1\omega + \mathrm{i}\varepsilon_3\omega\right), \\
L_{22} &= -P_1 - \Delta\omega - S_1\omega^2 + S_3\omega^4 - S_2\omega^3 - \omega\left(2\varepsilon_1 P_1 + \varepsilon_2 P_2\right) + \mathrm{i}\omega\left(2\varepsilon_3 P_1 + \varepsilon_5 P_2\right), \\
L_{23} &= \sqrt{P_1P_2}\left(-B - \varepsilon_2\omega + \mathrm{i}\varepsilon_4\omega + \mathrm{i}\varepsilon_5\omega\right), \quad L_{24} = \sqrt{P_1P_2}\left(-B - \varepsilon_2\omega + \mathrm{i}\varepsilon_4\omega\right), \\
L_{31} &= \sqrt{P_1P_2}\left(B - \varepsilon_2\omega\right), \quad L_{32} = \sqrt{P_1P_2}\left(B - \mathrm{i}\varepsilon_4\omega - \mathrm{i}\varepsilon_5\omega\right), \\
L_{33} &= P_2 + \Delta\omega + S_1\omega^2 - S_3\omega^4 - S_2\omega^3 - \omega\left(2\varepsilon_1 P_2 + \varepsilon_2 P_1\right) - \mathrm{i}\omega\left(\varepsilon_3 P_2 + \varepsilon_5 P_1\right), \\
L_{34} &= P_2\left(1 - \varepsilon_1\omega - \mathrm{i}\varepsilon_3\omega\right), \quad L_{41} = \sqrt{P_1P_2}\left(-B - \varepsilon_2\omega + \mathrm{i}\varepsilon_4\omega + \mathrm{i}\varepsilon_5\omega\right), \\
L_{42} &= \sqrt{P_1P_2}\left(-B - \varepsilon_2\omega\right), \quad L_{43} = P_2\left(-1 - \varepsilon_1\omega + \mathrm{i}\varepsilon_3\omega\right), \\
L_{44} &= -P_2 + \Delta\omega - S_1\omega^2 + S_3\omega^4 - S_2\omega^3 - \omega\left(2\varepsilon_1 P_2 + \varepsilon_2 P_1\right) + \mathrm{i}\omega\left(\varepsilon_3 P_2 + \varepsilon_5 P_1\right),
\end{aligned}$$

where $P_1 = 2P\cos^2(\phi)$ and $P_2 = 2P\sin^2(\phi)$, ϕ being the polarization angle.

Now for achieving the MI condition required for the generation of ultrashort pulses of the order of 500 fs and above, we follow a similar procedure as in case (i) of §3 to arrive at the dispersion relation from eq. (15) which is of the form

$$k = -S_2\omega^3 \pm \omega\sqrt{L_4 - 2\sqrt{L_5}} \tag{17}$$

where L_4 and L_5 have the same form as obtained in §3. Here too, the condition for instability to occur is $L_4^2 < 4L_5$ as is clear from eq. (17) and hence we obtain the same gain parameter as in case (i) of §3 even though the eigenvalues are different in both cases. Hence we can arrive at all the results considered in case (i) of §3. Likewise, we consider the remaining two cases present in §3 and numerically arrive at the same results as obtained in §3. We thus arrive at the conclusion that the modulational anstatz considered in eq. (14) can also effectively portray the MI phenomenon in the single-frequency propagation regime. Equation (15), being a linear homogenous differential equation, has a solution of the form

$$\mathbf{X}(\varsigma) = \exp(\mathrm{i}\mathbf{L}\varsigma)\,\mathbf{C} \tag{18}$$

where the constant column matrix $\mathbf{C}$ depends on the initial conditions of the four linearized side-band amplitudes. Figures 14 and 15 show the graphical relation for the Stokes and anti-Stokes side-band amplitudes respectively for the slow axis with respect to ς. For the Stokes case, $\omega = 2.0$ whereas for the anti-Stokes case, $\omega = 8.0$. Similar graphs can be obtained for the fast axis also.

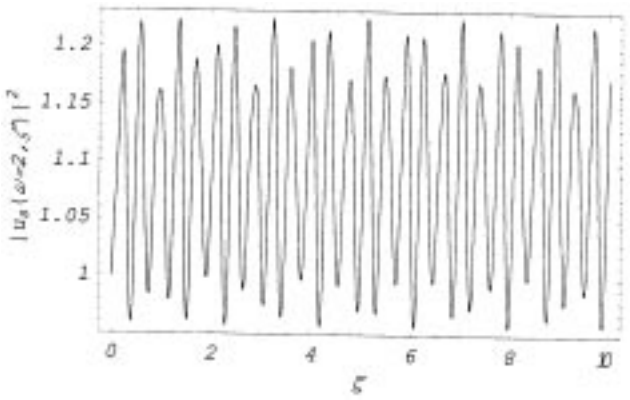

Figure 14. The intensity of the Stokes side-band amplitude for the slow axis for $\omega = 2.0$.

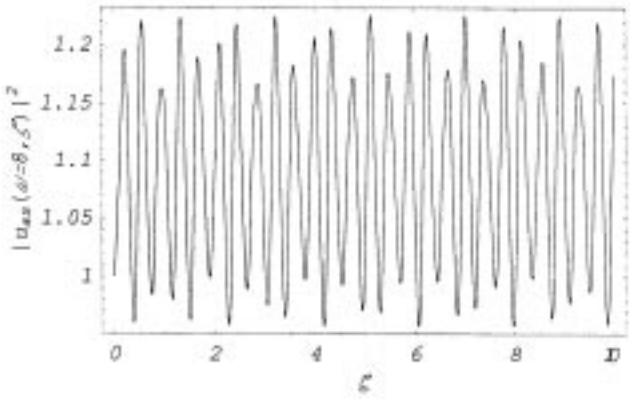

Figure 15. The intensity of the anti-Stokes side-band amplitude for the slow axis for $\omega = 8.0$.

5. Conclusions

We obtained conditions for the occurrence of cross-phase MI in the normal dispersion regime which occurs as a result of a group velocity mismatch between the linearly polarized eigenstates when the linearly polarized pump is oriented at 45° with respect to the slow or fast axis. We note that the instability conditions that govern the generation of ultrashort pulses for the three cases mentioned in §2 are not affected irrespective of the presence or absence of S_2, the dimensionless third-order dispersion coefficient. For variations in the pump polarization, maximum gain occurs for 45° polarization for all the cases considered in the article. The effect of SRS on MI is such that for comparative small values of the perturbation frequency, group velocity dispersion and cross-phase modulation terms dominate whereas for comparatively large values the perturbation frequency, the gain spectrum increases linearly with the result that the region of MI is widened due to SRS.

Moreover the self-steepening effect reduces the maximum gain and bandwidth. As one slowly approaches towards the zero group velocity dispersion regime, the condition for the cross-phase MI requires sufficiently large values of the total input power over a wide range of frequency detuning ω. At the zero group velocity dispersion regime, one obtains only the original MI. We have considered the perturbation amplitudes given by eq. (14) and have been able to retrieve all the results considered in §3 and thus the two methods discussed in §3 and §4 give the same values for the gain parameter.

Acknowledgements

The authors are thankful to M Lakshmanan and K Porsezian for valuable discussions. One of the authors (VCK) wishes to acknowledge the Associateship of IUCAA, Pune.

References

[1] G P Agrawal, *Nonlinear fiber optics* (Academic Press, New York, 1995)
[2] L A Ostrovskii, *Sov. Phys. JETP* **24**, 797 (1966)
[3] V I Karpman, *JETP Lett.* **6**, 277 (1967)
[4] Akira Hasegawa, *Phys. Rev. Lett.* **24**, 1165 (1970)
[5] Akira Hasegawa and W F Brinkman, *IEEE J. Quantum Electron.* **16**, 694 (1980)
[6] Akira Hasegawa and Yugi Kodama, *Solitons in optical communications* (Clarendon Press, Oxford, 1995)
[7] Nail N Akhmediev and Adrian Ankiewicz, *Solitons – nonlinear pulses and beams* (T J International Ltd., Great Britain, 1997)
[8] J R Taylor, *Optical solitons – theory and experiments* (Cambridge University Press, Cambridge, 1992)
[9] E Seve, P Tchofo Dinda, G Millot, M Remoissenet, J M Bilbault and M Haelterman, *Phys. Rev.* **A54**, 3519 (1996)
[10] P D Drummond, T A B Kennedy and J D Harvey, *Opt. Comm.* **78**, 137 (1990)
[11] R Ganapathy and V C Kuriakose, *Pramana – J. Phys.* **57**, 743 (2001)
[12] R Radhakrishnan and M Lakshmanan, *Phys. Rev.* **E54**, 2949 (1996)
[13] B A Malomed and R A Tasgal, *J. Nonlinear Opt. Phys. Mater.* **5**, 559 (1996)
[14] S B Cavalcanti, J C Cressoni, H R da Cruz and A S Gouveia-Neto, *Phys. Rev.* **A43**, 6162 (1991)
[15] Alexander V Buryak and Nail N Akhmediev, *Phys. Rev.* **E51**, 3572 (1995)
[16] Nail N Akhmediev, Alexander V Buryak and J M Soto-Crespo, *Opt. Comm.* **112**, 278 (1994)